Spray Coating Experiments: Setups and Methodologies

The latest eBook from Advanced Optical Metrology. Download for free.

Spray Coating Experiments: Setups and Methodologies, is the third in our Thin Films eBook series. This publication provides an introduction to spray coating, three article digests from Wiley Online Library and the latest news about Evident's Image of the Year Award 2022.

Wiley in collaboration with Evident, are committed to bridging the gap between fundamental research and industrial applications in the field of optical metrology. We strive to do this by collecting and organizing existing information, making it more accessible and useful for researchers and practitioners alike.

EVIDENT
OLYMPUS

WILEY

Enzyme-Photocatalyst Tandem Microrobot Powered by Urea for *Escherichia coli* Biofilm Eradication

Katherine Villa, Hanna Sopha, Jaroslav Zelenka, Martin Motola, Lukas Dekanovsky, Darya Chylii Beketova, Jan M. Macak, Tomáš Ruml, and Martin Pumera*

Urinary-based infections affect millions of people worldwide. Such bacterial infections are mainly caused by *Escherichia coli (E. coli)* biofilm formation in the bladder and/or urinary catheters. Herein, the authors present a hybrid enzyme/photocatalytic microrobot, based on urease-immobilized TiO_2/CdS nanotube bundles, that can swim in urea as a biocompatible fuel and respond to visible light. Upon illumination for 2 h, these microrobots are able to remove almost 90% of bacterial biofilm, due to the generation of reactive radicals, while bare TiO_2/CdS photocatalysts (non-motile) or urease-coated microrobots in the dark do not show any toxic effect. These results indicate a synergistic effect between the self-propulsion provided by the enzyme and the photocatalytic activity induced under light stimuli. This work provides a photo-biocatalytic approach for the design of efficient light-driven microrobots with promising applications in microbiology and biomedicine.

1. Introduction

Urinary tract infections are one of the most common afflictions caused by bacteria. It affects ≈150 million people per year worldwide.[1] Such types of infection are mainly associated with the presence of *Escherichia coli* (*E. coli*), which initiates the infection from the periurethral area to the urethra and finally colonizes the bladder.[1] Once there, bacteria can adhere to the walls, leading to biofilm formation. This cannot only occur in the bladder but also into indwelling urinary catheters.[2,3] Since bacterial biofilms are protected by a polymeric matrix, they exhibit a high resistivity against antibiotics, neutrophils, and physical or chemical stresses.[2,4,5] As a result, biofilm-mediated infections are more difficult to treat, leading to chronic bacterial infections that cannot be easily eliminated by conventional antibiotic therapy.[4] Therefore, the development of efficient antibiofilm treatments remains a priority.

Different approaches dealing with bacterial biofilm inactivation have been developed over the last years, including liposomes and polymer-based drug delivery vehicles and application of external fields such as ultrasound, electrical, and light.[6–8] Recently, these strategies have been combined with self-propelled micro/nanorobots that convert energy from the environment into mechanical energy. Because of their active motion, these devices can increase penetrability into the biofilm, leading to a higher dispersibility of antimicrobial agents in comparison with passive particles. Among the diverse types of micro/nanorobots that have been investigated so far for biofilm removal belong to magnetotactic biohybrids,[9] and to catalytic,[10–12] thermophoretic,[13] magnetic,[14,15] and dual catalytic/magnetic micro/nanomachines.[16] In particular, light-based technologies hold great promise for therapeutic approaches,

K. Villa, L. Dekanovsky, M. Pumera
Center for Advanced Functional Nanorobots
Department of Inorganic Chemistry
University of Chemistry and Technology Prague
Technická 5, Prague 166 28, Czech Republic
E-mail: martin.pumera@vscht.cz
H. Sopha, M. Motola, D. C. Beketova, J. M. Macak
Center of Materials and Nanotechnologies
Faculty of Chemical Technology
University of Pardubice
Náměstí čs
Legií 565, Pardubice 530 02, Czech Republic

H. Sopha, J. M. Macak, M. Pumera
Central European Institute of Technology
Brno University of Technology
Purkyňova 123, Brno 612 00, Czech Republic
J. Zelenka, T. Ruml
Department of Biochemistry and Microbiology
University of Chemistry and Technology Prague
Technická 5, Prague 166 28, Czech Republic
M. Pumera
Department of Medical Research
China Medical University Hospital
China Medical University
No. 91 Hsueh-Shih Road, Taichung 40402, Taiwan
M. Pumera
Department of Chemical and Biomolecular Engineering
Yonsei University
50 Yonsei-ro
Seodaemun-gu, Seoul 03722, Korea

ⓘ The ORCID identification number(s) for the author(s) of this article can be found under https://doi.org/10.1002/smll.202106612.

due to the possibility of localized and controlled treatment in a non-invasive way. Therefore, the development of hybrid photo-biocatalytic micro/nanorobots that harvest biochemical energy from the environment for self-propulsion with simultaneous release of highly reactive species represents an efficient and biocompatible strategy to remove biofilm-based infections.

Titanium dioxide is a benchmark photocatalyst for a wide range of applications, ranging from environmental,[17] energy[18,19] to biomedical applications.[20,21] This material exhibits a high (photo-)chemical stability, non-toxic, low cost, and strong oxidative behavior.[22] Owing to its unique properties, TiO_2 has been the most common photoactive component of light-driven micro/nanorobots.[23] However, it usually requires noble metals or a high concentration of toxic fuels for efficient propulsion,[24–26] which limits its application in the biomedical field. Previous studies have demonstrated that TiO_2-based nanotube bundles stand as a versatile, smart, and biocompatible platform for tissue engineering, drug delivery, and biosensing.[20] Although there are a few works on microrobots based on TiO_2 nanotube bundles,[27,28] these require UV photoactivation, a high concentration of H_2O_2 (10% wt.), and/or surfactants. Therefore, it is necessary to explore alternative biocompatible strategies for triggering their motion, while taking advantage of their fast light response, highly oxidative capability, and large surface area. The coupling of TiO_2 with visible-light-responsive materials, such as CdS, is a straightforward approach to fabricate photocatalytic-based microrobots that can be activated under visible light with improved electron–hole separation. Herein, we present urease-coated photocatalytic microrobots that can self-propel in urea. Upon photoactivation with visible light, the photocatalytic counterpart, based on TiO_2/CdS nanotube bundles, generate reactive radicals that cause phototoxic effect on the surface of the biofilm. As a proof-of-concept, we used the as-developed enzyme-photocatalyst tandem microrobots for removal of *E. coli* biofilm. Such hybrid microrobots open the door for future applications in the desinfection of urinary catheters or bladder-related biofilm infections.

2. Results and Discussion

The hybrid photocatalytic microrobots, consisting of a scaffold of TiO_2/CdS nanotube bundles, were fabricated by anodization of a titanium foil, as shown in **Figure 1**. After anodization, the TiO_2 nanotube layers were etched to TiO_2 bundles, followed by calcination at high temperature (400 °C for 1 h) to induce the formation of the anatase phase, which is one of the most photoactive crystalline phases of TiO_2.[29,30] To provide them with a visible light response, these nanotube bundles were decorated with CdS nanoparticles (NPs) using colloidal synthesis based on oleic acid approach (details in the Experimental part). Figure S1A, Supporting Information, corroborates the light absorption capabilities of the TiO_2/CdS in the visible range. Moreover, the fluorescence spectrum shown in Figure S1B, Supporting Information, is in agreement with the one reported for TiO_2/CdS heterostructures in the literature.[31] Upon the release of the TiO_2/CdS nanotube bundles, they were functionalized with urease to obtain enzyme/photocatalytic tandem microrobots, named U-μrobots. The resulting U-μrobots exhibit a dual response: i) photocatalytic activation under visible light irradiation that results in the generation of reactive oxidizing species (ROS); and ii) self-propulsion due to the enzymatic decomposition of urea by the urease attached on the surface. Considering that the formation of *E. coli* biofilm in the bladder and onto urinary-based catheters is a common cause of urinary infections, we investigated as proof-of-concept the capabilities of these hybrid U-μrobots for eradication of this type of bacterial biofilm in the presence of urea, which is a common compound found in such environments.

Figure 2 shows the structural and morphological characterization of the hybrid microrobots. Figure 2A shows the SEM image of different U-μrobots that exhibit a length of ≈15 μm and a width of ≈5 μm. Figure 2B shows a representative image of U-μrobots that consist of nanotube bundles with a nanotube diameter of ≈130 nm decorated with CdS NPs. As shown in the insets, one side of these nanotubes presents open holes (Figure 2C) while the other side is closed (Figure 2D). A high magnification STEM image shows that the CdS NPs are not only present on the surface of the TiO_2 nanotube bundles but also within the nanotubes (Figure 2E). The size of deposited CdS NPs was found to be ≈50 nm (Figure 2F). The EDX-Mapping images illustrated in Figure 2E confirm the composition of the microrobots, including Ti, O, Cd, and S. Upon enzyme loading, the presence of C and N from the urease can also be observed in Figure S2, Supporting Information.

Additionally, an XRD of the microrobots is included in Figure S3, Supporting Information. The diffraction patterns
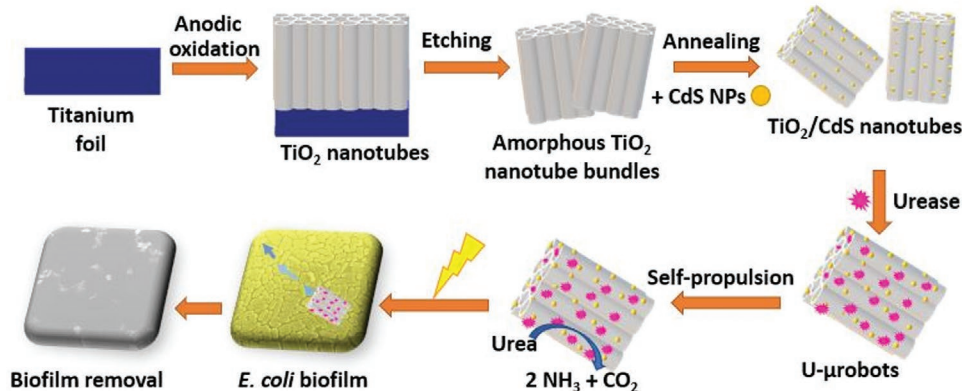

Figure 1. Schematic illustration of the fabrication of hybrid photocatalytic TiO_2/CdS microrobots functionalized with urease (U-μrobots) for the removal of *E. coli* biofilm.
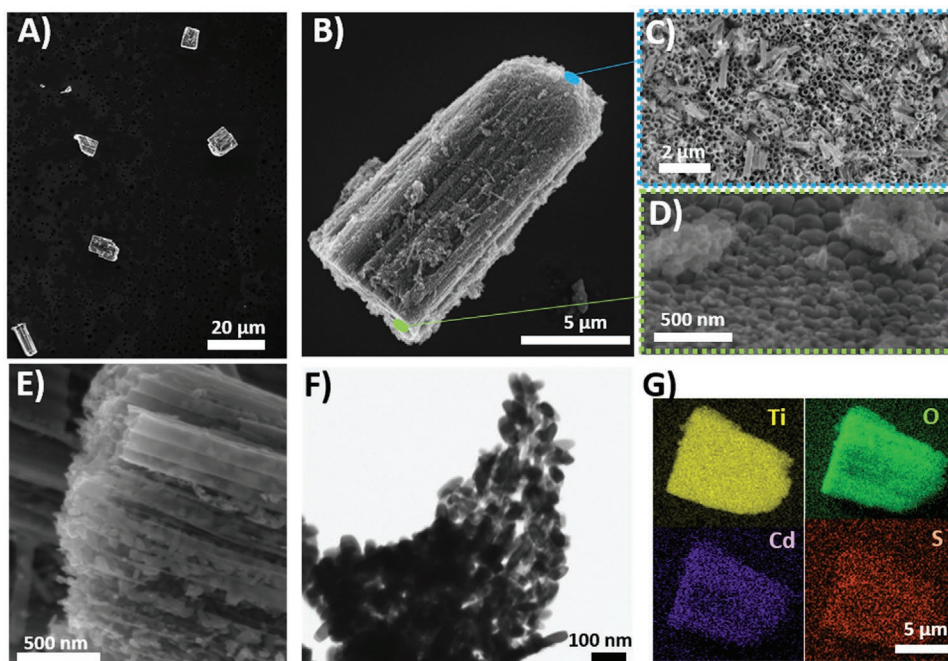
Figure 2. Characterization of the U-μrobots. A) SEM image of different microrobots. B) SEM image of a single microrobot, blue inset C) showing open holes in one end of the microrobot and the green inset D) correspond to the opposite end. E) STEM HAADF image of a microrobot showing the nanotubes homogenously decorated with CdS NPs. F) STEM bright-field image of TiO$_2$/CdS nanotube bundles. G) EDX-Mapping characterization of the microrobots showing the presence of Ti, Cd, O, and S.

correspond to the anatase crystalline phase of TiO$_2$ (PDF-4+: 00-021-1272).[30,32] Moreover, a peak located at a 2θ value of 29.7° can be attributed to CdS (PDF-4+: 00-041-1049).[33]

The motion characterization of the U-μrobots was evaluated by assessing their motion capabilities at different concentrations of urea. As can be seen from Videos S1 and S2, Supporting Information, the U-μrobots mainly move by following straight trajectories. **Figure 3**A shows the average speeds of the U-μrobots swimming at 50, 100, 200, and 300 mM of urea. A maximum speed of 3.3 ± 0.3 μm s^{-1} was obtained with a 50 mM solution, which is comparable with other reported urease-powered tubular nanomotors.[34] Since there were not any statistically significant differences upon the increase of the urea concentration, which is attributed to the activity kinetics of urease,[34] a solution of 50 mM of urea was selected as the optimal concentration for the biofilm removal tests. The motion characterization of the microrobots at concentrations of urea lower than 50 mM is included in Figure S4, Supporting Information.

The urease activity of the enzyme immobilized onto the microrobots was calculated from the calibration curve included in Figure S5, Supporting Information. It was found to be 111 units/L, indicating that upon immobilization onto the surface of the TiO$_2$/CdS nanotube bundles, the urease is still active. The motion mechanism is attributed to the enzymatic conversion of urea into ammonia and carbon dioxide that leads to a concentration gradient, driving the microrobot by self-diffusiophoresis.[34–36] In a previous work, it was found that the presence of urease inside the cavity of the tubular microrobots is key to achieve directional motion, which is enhanced by the urease loaded on the outer surface.[34] Since we did not modify the surface of the microrobots to selectively bind the urease in

the inner or outside surface, it is expected that the enzyme is present in both sides.

As the next step, we evaluated the antibiofilm capabilities of the U-μrobots in the dark and under light irradiation. For comparison, we also tested the respective blanks including control (no treatment), urea (no U-μrobots), TiO$_2$/CdS nanotube bundles (non-motile), TiO$_2$/CdS nanotube bundles (non-motile) + urea, U-μrobots, and U-μrobots + urea. Figure 3B represents the performance of each group under visible-light irradiation. The blank experiment evidences that the light source used in this study did not cause any detrimental effect on the viability of the biofilm. On the other hand, pure urea exhibited a slightly detrimental effect on the biofilm density, while the presence of TiO$_2$/CdS nanotube bundles (non-motile) combined with urea showed an increase of the biofilm density. This unexpected behavior might be attributed to the fact that urea can be decomposed by photocatalytic reactions,[37] leading to a lower amount of urea that results in a lower toxicity to the biofilm. In contrast, a slight decrease was observed in the presence of TiO$_2$/CdS nanotube bundles (non-motile) with water under light irradiation, which can be attributed to the photoactivation of the photocatalyst that involves the generation of reactive radicals.[38,39] Overall, the highest removal efficiency was obtained with the U-μrobots in the presence of urea under light irradiation, whereas in the dark, the effect was minimal (Figure S6, Supporting Information).

The effect of different concentrations of U-μrobots on the biofilm viability was also assessed (Figure S7, Supporting Information). By increasing the concentration of U-μrobots from 0.05 to 0.5 mg ml^{-1}, the biofilm viability decreased proportionally. Overall, the high antimicrobial activity can be attributed to the combined effect of the photocatalytic/enzymatic properties of the U-μrobots.
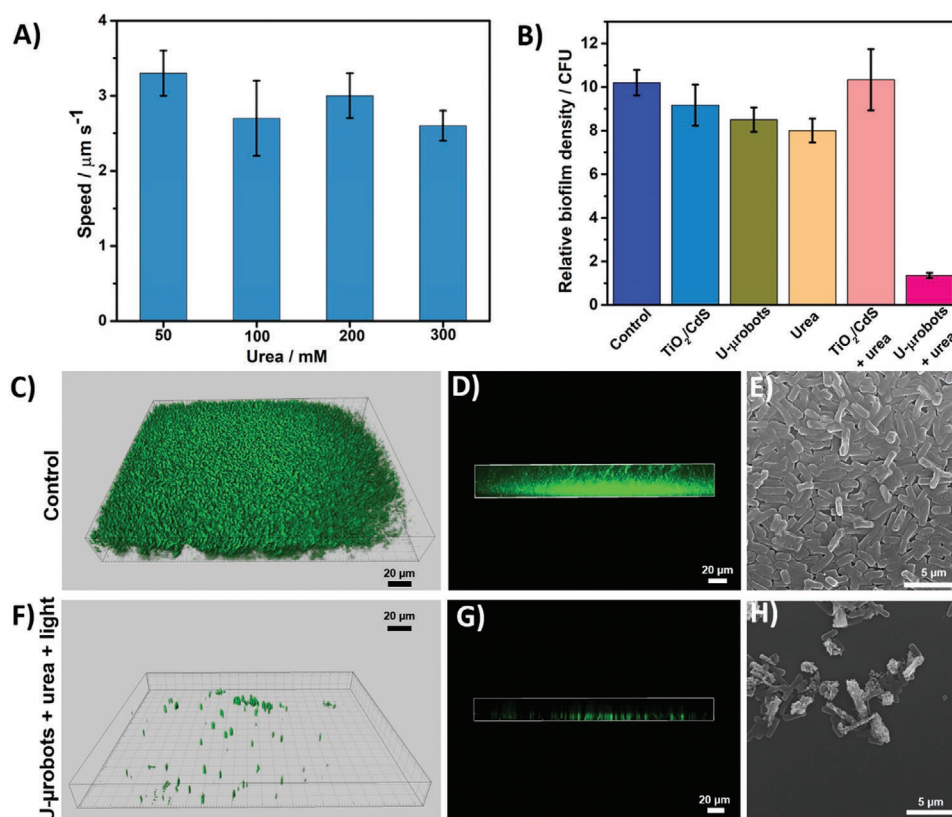
Figure 3. *E. coli* biofilm removal. A) Motion speed of the μrobots at different urea concentrations ($n = 20$; error bars represent the standard error of the mean). B) *E.coli* biofilm removal tests, including the respective controls and the U-μrobots with and without urea under light irradiation ($n = 6$; error bars represent the standard error of the mean). C,D) Confocal microscope images of the biofilm before and F,G) after treatment the microrobots in the presence of urea and light. E) SEM image before and H) after treatment with the microrobots in the presence of urea and light.

The generation of ammonia, due to the hydrolysis of urea, has been demonstrated to have a negative effect on bacterial biofilm.[11] However, the fact that the U-μrobots in a combination of urea in the dark did not show any toxic effect on the biofilm, suggests that the ammonia generated by the enzymatic activity of urease immobilized on our microrobots was not enough to disrupt the biofilm. Previous works have demonstrated that the photoactivation of a photocatalyst in the presence of an enzyme can lead to a photo-biocatalytic synergy, in which the photogenerated electrons are transferred to the enzyme.[40,41] In our configuration, urea may act as a hole scavenger, while the photogenerated electrons on the TiO$_2$/CdS photocatalyst may be directly transferred to the urease, due to the close contact, enhancing its activity. Likewise, the electron–hole recombination is diminished, leading to an improvement over the whole photocatalytic activity of the system. Considering that visible light is not able to penetrate deep in tissues, a foreseen potential application of visible-light photoactivated enzyme-coated microrobots would involve light-based technologies, in which the urinary catheters can be provided with optical fibers[2,42] to activate the microrobots while swimming in biocompatible fuels available at the bladder.

Complementarily, the morphology and density of the biofilm, before and after treatment with the U-μrobots, was also characterized by SEM and confocal laser scanning microscopy (CLSM), respectively. As can be seen from Figure 3C–E, the biofilm consists of a high density of *E. coli*, forming a compact layer. Upon illumination in the presence of the U-μrobots, most of the biofilm was removed (Figure 3F,G), the remaining was only a few cells attached to the U-μrobots (Figure 3H). Moreover, the biofilm structure evidenced that the untreated sample consists of several layers of bacteria (Figure S8, Supporting Information), while upon treatment, only a few remaining bacteria were observed in the surface layers (Figure S9, Supporting Information).

Considering that the generation of ROS by the photocatalyst may affect the urease activity, additional experiments evaluating the ROS generation and urease activity under light irradiation were carried out. As shown in **Figure 4**A, the photogeneration of ROS increased over time, reaching values considerably higher than in the dark, which is in agreement with the photocatalytic behavior of U-μrobots. Therefore, the urease-coating did not negatively affect the photocatalytic activity of the U-μrobots. On the other hand, there was a slight decrease of urease activity after 30 min of light irradiation (Figure 4B), indicating that the presence of ROS may oxidize to some extent the thiol groups from the urease,[43,44] without leading to its full deactivation. These results suggest that both enzymatic/photocatalytic components can maintain their activity under light irradiation, contributing to an efficient bacterial biofilm removal.

On the other hand, to detect morphological changes on the remaining *E. coli* cells, the samples containing the microrobots were further characterized by SEM and STEM (**Figure 5**). Upon treatment, there were evident changes of cell disruption.

**ADVANCED
SCIENCE NEWS**

www.advancedsciencenews.com
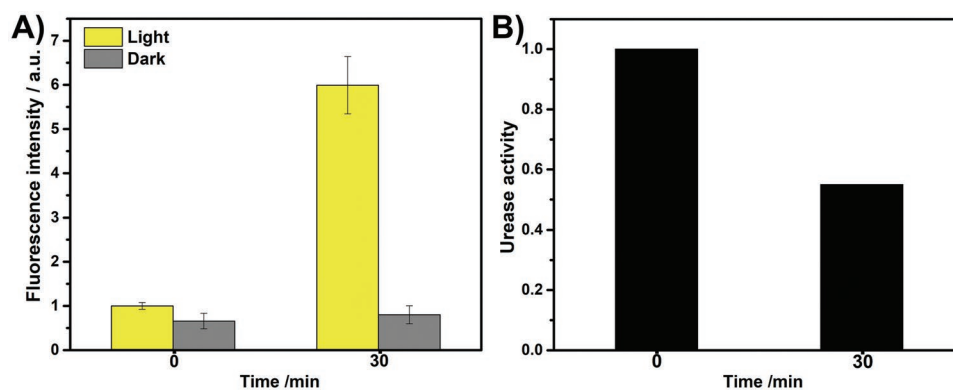
NANO · MICRO

small

www.small-journal.com

Figure 4. Photocatalytic and enzymatic activity of the microrobots. A) ROS generation measured as oxidation of dihydrorhodamine 123 probe ($n = 4$; error bars represent the standard error of the mean) and B) urease activity measured under the same conditions by indophenol assay.

For instance, the leaking of the intracellular content, due to the destruction of the membrane cell,[45,46] resulted in dead cells with a flat shape (Figure 5A). In addition, we have measured the release of lactate dehydrogenase (LDH) upon treatment, which is an indicator of cell death, related with cell membrane disruption.[47] As shown in Figure S10, Supporting Information, the highest LDH releasement was achieved by the microrobots under light irradiation, evidencing their photoinduced bactericidal capabilities. Furthermore, bacteria shrinkage and formation of dents (indicated by white arrows) are also evidenced in Figure 5B. Such effects including membrane disruption by photocatalytic metal oxides, such as TiO_2, are usually associated with the generation of ROS[21,48,49] or direct interaction of the metal-based components with the cell membrane.[50]

TiO_2-based nanotube bundles have previously been investigated for drug delivery and therapeutic treatments, showing promising efficiencies due to their high loading capacity inside the nanotubes, controllable pore, and self-ordered structure.[20,51] Any possible toxicity of our U-µrobots under potential real applications could be avoided by optimizing the size of the particles, one-direction flow of the urine, the protection of the cells by a mucous layer, and an intended short-term contact

of the microrobots with cells. It should be noted that the short term toxicity of U-µrobots to human fibroblasts was found to be negligible (Figure S11, Supporting Information). Further research should be devoted to decrease their size and decoration with plasmonic nanoparticles such as Au NPs to achieve their photoactivation under NIR light with no side effects.

3. Conclusions

We have fabricated nanostructured TiO_2/CdS photocatalytic microrobots consisting of TiO_2 nanotube bundles, decorated with CdS NPs. These microrobots exhibit a crystalline structure and visible light absorption. The immobilization of urease on their structure provided them with an additional catalytic ability for triggering their autonomous motion in the presence of urea. For which the enzymatic activity of the urea attached on their surface was confirmed. These hybrid microrobots were able to efficiently disrupt *E. coli* biofilm after 2 h of visible light irradiation, due the combined effect of self-propulsion along with the simultaneous generation of ROS. Complementarily, the biofilm eradication, and cell disruption were evidenced by confocal and SEM/STEM microscopy characterization and LDH releasement. The enzymatic activity, upon generation of reactive radicals by the photocatalyst in the presence of light, was maintained, evidencing that both components can work all together. Overall, this work demonstrates the potential of combining enzyme/photocatalytic components within the same microrobot structure for the efficient removal of a bacterial biofilm. Thus, it provides an alternative strategy for developing advanced photoresponsive microrobots with improved catalytic activity, offering great potential for the future applications of micromachines.
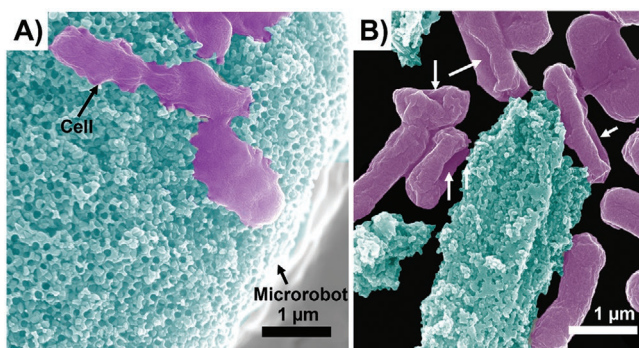

Figure 5. High-resolution SEM images of the microrobots after treatment. A) False-colored SEM image of dead *E. coli* bacteria cells attached on the surface of the U-µrobots, showing apoptosis features and B) false-colored SEM image of remaining bacteria cells upon treatment with the U-µrobots (white arrows indicate dent formation). The SEM images were artificially colored to distinguish the surface of the microrobots and the damaged *E. coli* bacteria cells.

4. Experimental Section

Fabrication of U-µrobots: TiO_2 nanotube layers of ≈20 µm thickness were produced by anodization, as described earlier.[52] Briefly, Ti foils (Sigma-Aldrich, 127 µm thick) were degreased in isopropanol and acetone by sonication for 1 min, respectively, rinsed with isopropanol and dried in air. The anodization of the Ti foils was carried out in an ethylene glycol-based electrolyte containing 1.5 vol% H_2O and 170 mm

NH$_4$F, using the Ti foil as anode and a Pt foil as cathode, at 60 V for 4 h. After anodization, the TiO$_2$ NT layers were cleaned from the electrolyte by sonication in isopropanol for 15 min.

To obtain TiO$_2$ NT bundles, a selective chemical etching treatment of the TiO$_2$ NT layers was conducted. First, the prepared TiO$_2$ NT layers were pre-annealed at 150 °C for 1 h in air. Second, the layers were immersed in a piranha solution (H$_2$SO$_4$:H$_2$O$_2$ = 3:1) for 5 min at 70 °C and subsequently sonicated (FB11203, Fisherbrand) in isopropanol for 30 min at 37 kHz and 100% power. Finally, the prepared TiO$_2$ nanotube bundles were separated from the isopropanol solution by centrifugation (Optima MAX-XP, Beckman Coulter) at 5000 rpm for 10 min at 25 °C using a fixed angle rotor MLA-50. To transform the amorphous TiO$_2$ nanotube bundles to the crystalline anatase phase, the TiO$_2$ nanotube bundles were annealed in a porcelain crucible in a muffle oven at 400 °C for 1 h (heating rate: 2.1 °C min^{-1}) before further use. Further experimental details and practical examples of this procedure can be found in a previous publication.[53]

The synthesis of CdS NPs was based on the approaches using oleic acid and oleylamine for the synthesis of Cd-chalcogenide NPs[54–56] and optimized for CdS colloidal synthesis. In brief, two precursor solutions of Cd-oleylamine and S-oleylamine, each, were prepared at a ratio of Cd:S = 1:10. The Cd-oleylamine was prepared by adding 0.12 mL oleic acid (tech. grade, 90%, Sigma), 1.5 mL oleylamine (tech. grade, 70%, Sigma), and 1.38 mL 1-octadecene (tech. grade, 90%, Sigma) to 0.0192 g CdCl$_2$. The solution was heated in a closed vial to 150 °C under constant mixing using magnetic stirring until the CdCl$_2$ was dissolved and a transparent solution of Cd-oleylamine was formed. The S-oleylamine solution was prepared by adding 1.5 mL oleylamine and 0.5 mL 1-octadecene to 0.0346 g S. The mixture was heated in a closed vial at 150 °C until a complete dissolution. The color of the solution changed from yellow to red due to a formation of S-oleylamine.

TiO$_2$ nanotube bundles were given in a reactor glass vessel with a protective steel cover (Buchiglasuster, Switzerland) containing 0.04 mL/1 mg TiO$_2$ nanotube bundles of each precursor solution and 3 mL 1-octadecene. The solution was purged with N$_2$ for 30 min for deaeration. Afterward, the reactor vessel was sealed with a lid and placed in molten Wood alloy, which was used as a thermal bath liquid. The synthesis was carried out at 250 °C for 2 h. After the reaction the solution had orange color, indicating the formation of CdS. At the end, the reactor vessel was removed from the Wood alloy and cooled down in the air. The TiO$_2$ nanotube bundles were removed from the reactor tube and washed with acetone and heptane, respectively, until the washing solution was colorless. Finally, the modified TiO$_2$ nanotube bundles were placed into the vacuum oven at 150 °C overnight to remove organic residues.

Urease functionalization of the microrobots was performed by following a procedure reported elsewhere with some minor modifications.[34] In brief, the surface of the microrobots was first modified with APTES (3-aminopropyltriethoxysilane) followed by mixing with a glutaraldehyde solution for 3 h. Upon washing with PBS, the microrobots were then suspended in a urease solution (3 mg mL^{-1}) and left it overnight under shaking. Finally, the urease functionalized TiO$_2$/CdS microrobots (U-µrobots) were collected by centrifugation and washed with MilliQ water 3 times.

Characterization of the As-Synthesized U-µrobots: The crystalline structure of the microrobots was determined by X-ray powder diffraction (XRD) using a Bruker D8 Discoverer diffractometer with parafocusing Bragg–Brentano geometry and Cu Kα radiation source. The UV–vis absorbance spectrum was measured using a Jasco V-750 UV–Visible spectrophotometer equipped with an integrating sphere and the fluorescence measurements were conducted in a Jasco FP 8550 spectrofluorometer, using a 0.1 mg mL^{-1} TiO$_2$/CdS nanotubes suspension in ultrapure water. The morphological features were examined with a SEM/STEM Tescan Maia3 microscope equipped with an energy-dispersive X-ray (EDX, Oxford Instruments) detector. The enzymatic activity of the urease attached to the surface of the microrobots was determined with a commercial urease activity kit (Sigma-Aldrich). The concentration of the U-µrobots used for the experiments was 1 mg mL^{-1}. It consisted of the quantification of the ammonia generated by the hydrolysis of urea, which is catalyzed by urease. The resulting ammonia was determined by measuring the absorbance at 670 nm with a UV–Vis microplate spectrophotometer (Multiskan Sky, Thermo Scientific).

The motion characterization of the U-µrobots was performed by using an inverted optical microscope (Olympus IX73) equipped with a camera (Retiga R1 CCD) with Ocular software, as described as follows: a suspension of the microrobots was placed onto a glass slide and different concentrations of urea were added (50–300 mm). The speed was calculated by tracking the motion trajectories of the microrobots with a NIS Elements tracking software.

E. coli Biofilm Formation: E. coli was obtained from the collection of Yeasts and Industrial Microorganisms (DBM) at UCT Prague. It was cultured in Luria-Bertani (LB) medium at 37 °C and stored on LB agar at 4 °C. The biofilm was prepared in polystyrene 96-well plates at 37 °C overnight using medium inoculated with E. coli at O.D. 1 McFarland.

Experiments of Biofilm Removal by U-µrobots: The medium over the biofilm was aspired and replaced either by sterile water or by a solution of urea (50 mm). Then, the TiO$_2$/CdS nanotube bundles (non-enzyme-coated) or U-µrobots were added in the indicated concentration (0.5 mg mL^{-1} if not stated otherwise). The samples were subsequently incubated for 120 min either in dark or illuminated with a water-filtered white halogen light (18 mW cm^{-2}). Then the liquid was aspired and replaced by sterile water. The biofilm was disintegrated by vigorous pipetting and ultrasonication. The released cells were serially diluted, and their concentration was determined by Miles and Misra cultivation method on LB agar.

E. coli Biofilm Imaging: The imaging of the E. coli biofilm, before and after treatment, was performed by SEM/STEM and spinning disc confocal microscopy. Prior to the SEM/STEM imaging, the biofilm samples were first fixed with a solution containing formaldehyde (2%) and glutaraldehyde in phosphate buffer (2.5%, pH = 7.4) for 2 h at 24 °C. Then, the samples were dehydrated with an increasing concentration of ethanol (50%, 70%, 80%, and 90%). After that, a thin layer of platinum (5 nm) was sputtered on the samples for subsequent SEM/STEM characterization. In parallel, spinning disc confocal microscopy was performed with Andor revolution xD microscope on Olympus IX81 platform and operated with iQ3 software (Andor ltd). Live bacteria were stained with SYTO9 probe and images taken at 488 nm excitation laser and 525 nm emission filter. Images were processed with Imaris software.

Detection of Reactive Oxygen Species: E. coli culture was treated with dihydrorhodamine 123 probe (DHR) and illuminated with white light. DHR oxidized by released ROS was detected at 488/525 nm using spectrofluorimetry.

Lactate Dehydrogenase (LDH) Release: E. coli culture was treated in the same way as during biofilm removal measurement. LDH release into culture medium was detected using lactate dehydrogenase assay kit by Merck.

Cell Culture and Toxicity: Human fibroblast cells (MRC-5, ATCC) were cultivated in the EMEM medium supplemented with 0.5 mm glutamine, 5% fetal bovine serum, and 1% antibiotic antimycotic solution at 37 °C in an incubator with 5% CO$_2$ atmosphere and 90% humidity. The cells were seeded 24 h before the experiment in the 96-well plate. The cells were exposed to the nanorobot suspension in the different concentrations for 30 min. After exposure, the media were changed for the fresh one and cells were cultivated for 3 days. Viability of cells was measured by resazurin assay.

Supporting Information

Supporting Information is available from the Wiley Online Library or from the author.

Acknowledgements

Conflict of Interest

The authors declare no conflict of interest.

Author Contributions

K.V. designed the experiments and performed the characterization of the microrobots and wrote the first draft of the manuscript. J.Z. performed the biofilm removal tests and the respective imaging by confocal microscopy. L.D. performed SEM and STEM characterization of the biofilm and microrobots. H.S. designed and fabricated TiO_2 nanotubes, M.M. prepared TiO_2 nanotube bundles, D.C.B. provided CdS decoration to realize the final TiO_2/CdS microarrays. T.R. supervised the biological part of the research. J.M.M. and M.P. supervised the research. All authors have contributed to the writing and they have given approval to the final version of the manuscript.

Data Availability Statement

The data that support the findings of this study are available from the corresponding author upon reasonable request.

Keywords

[1] A. L. Flores-Mireles, J. N. Walker, M. Caparon, S. J. Hultgren, *Nat. Rev. Microbiol.* **2015**, *13*, 269.

[2] T. L. Vollmerhausen, A. Conneely, C. Bennett, V. E. Wagner, J. C. Victor, C. P. O'Byrne, *J. Photochem. Photobiol. B* **2017**, *170*, 295.

[3] L. E. Nicolle, *Antimicrob. Resist. Infect. Control* **2014**, *3*, 23.

[4] G. G. Anderson, J. J. Palermo, J. D. Schilling, R. Roth, J. Heuser, S. J. Hultgren, *Science* **2003**, *301*, 105.

[5] J. W. Costerton, P. S. Stewart, E. P. Greenberg, *Science* **1999**, *284*, 1318.

[6] a) W. C. de Melo, P. Avci, M. N. de Oliveira, A. Gupta, D. Vecchio, M. Sadasivam, R. Chandran, Y.-Y. Huang, R. Yin, L. R. Perussi, G. P. Tegos, J. R. Perussi, T. Dai, M. R. Hamblin, *Expert Rev. Anti-Infect. Ther.* **2013**, *11*, 669; b) J. Li, C. C. Mayorga-Martinez, C. D. Ohl, M. Pumera, *Adv. Funct. Mater.* **2021**, *32*, 2102265.

[7] M. Erriu, C. Blus, S. Szmukler-Moncler, S. Buogo, R. Levi, G. Barbato, D. Madonnaripa, G. Denotti, V. Piras, G. Orrù, *Ultrason. Sonochem.* **2014**, *21*, 15.

[8] J. L. Del Pozo, M. S. Rouse, R. Patel, *Int. J. Artif. Organs* **2008**, *31*, 786.

[9] a) M. M. Stanton, B.-W. Park, D. Vilela, K. Bente, D. Faivre, M. Sitti, S. Sánchez, *ACS Nano* **2017**, *11*, 9968; b) C. C. Mayorga, J. Zelenka, J. Grmela, H. Michalkova, T. Ruml, J. Mareš, M. Pumera, *Adv. Sci.* **2021**, *8*, 2101301.

[10] a) J. Wang, W. Gao, *ACS Nano* **2012**, *6*, 5745; b) K. Villa, J. Viktorova, J. Plutnar, T. Ruml, L. Hoang, M. Pumera, *Cell Rep. Phys. Sci.* **2020**, *1*, 100181.

[11] a) M. Ussia, M. Urso, K. Doleželíková, H. Michálková, V. Adam, M. Pumera, *Adv. Funct. Mater.* **2021**, *31*, 2101178; b) D. Vilela, N. Blanco-Cabra, A. Eguskiza, A. C. Hortelao, E. Torrents, S. Sanchez, *ACS Appl. Mater. Interfaces* **2021**, *13*, 14964.

[12] Z. Lin, C. Gao, D. Wang, Q. He, *Angew. Chem., Int. Ed.* **2021**, *133*, 8832.

[13] T. Cui, S. Wu, Y. Sun, J. Ren, X. Qu, *Nano Lett.* **2020**, *20*, 7350.

[14] G. Hwang, A. J. Paula, E. E. Hunter, Y. Liu, A. Babeer, B. Karabucak, K. Stebe, V. Kumar, E. Steager, H. Koo, *Sci. Rob.* **2019**, *4*, eaaw2388.

[15] a) Y. Dong, L. Wang, K. Yuan, F. Ji, J. Gao, Z. Zhang, X. Du, Y. Tian, Q. Wang, L. Zhang, *ACS Nano* **2021**, *15*, 5056; b) H. Zhou, C. C. Mayorga-Martinez, S. P. , L. Zhang, M. Pumera, *Chem. Rev.* **2021**, *121*, 4999.

[16] K. Yuan, B. Jurado-Sánchez, A. Escarpa, *Angew. Chem., Int. Ed.* **2021**, *60*, 4915.

[17] a) W. Gao, J. Wang, *ACS Nano* **2014**, *8*, 4, 3170; b) B. Jurando-Sánchez, J. Wang, *Environ. Sci.: Nano* **2018**, *5*, 1530; c) L. Kong, A. Ambrosi, M. Z. M. Nasir, J. Guan, M. Pumera, *Adv. Funct. Mater.* **2019**, *29*, 1903872; d) Y. Ying, M. Pumera, *Chem. - Eur. J.* **2019**, *25*, 106; e) L. Wang, K. Villa, *Environ. Sci.: Nano* **2021**, *8*, 3440; f) C. M. Oral, M. Ussia, D. K. Yavuz, M. Pumera, *Small* **2022**, https://doi.org/10.1002/smll.202106271.

[18] a) M. P. Browne, V. Urbanova, J. Plutnar, F. Novotný, M. Pumera, *J. Mater. Chem. A* **2020**, *8*, 1120; b) K. Villa, J. R. Galán-Mascarós, *ChemSusChem* **2021**, *14*, 2023; c) X. Zhou, I. Hwang, O. Tomanec, D. Fehn, A. Mazare, R. Zboril, R. Meyer, P. Schmuki, *Adv. Funct. Mater.* **2021**, *31*, 2102843.

[19] a) K. Villa, J. R. Galán-Mascarós, N. López, E. Palomares, *Sustainable Energy Fuels* **2021**, *5*, 4560; b) S. Hejazi, S. Mohajernia, B. Osuagwu, G. Zoppellaro, P. Andryskova, O. Tomanec, S. Kment, R. Zbořil, P. Schmuki, *Adv. Mater.* **2020**, *32*, 1908505.

[20] G. G. Genchi, Y. Cao, T. A. Desai, in *Smart Nanoparticles for Biomedicine* (Ed: G. Ciofani), Elsevier, New York **2018**, pp. 143–157.

[21] M. Kalbacova, J. M. Macak, F. Schmidt-Stein, C. T. Mierke, P. Schmuki, *Phys. Status Solidi RRL* **2008**, *2*, 194.

[22] K. Nakata, A. Fujishima, *J. Photochem. Photobiol. C* **2012**, *13*, 169.

[23] a) L. Kong, C. C. Mayorga-Martinez, J. Guan, M. Pumera, *Small* **2020**, *16*, 1903179; b) J. Li, M. Pumera, *Chem. Soc. Rev.* **2021**, *50*, 2794; c) J. Zhang, J. Song, F. Mou, J. Guan, A. Sen, *Trends Chem.* **2021**, *3*, 387.

[24] a) S. K. Srivastava, M. Guix, O. G. Schmidt, *Nano Lett.* **2016**, *16*, 817; b) R. Dong, Q. Zhang, W. Gao, A. Pei, B. Ren, *ACS Nano* **2016**, *10*, 839.

[25] a) G. Zhao, M. Viehrig, M. Pumera, *Lab Chip* **2013**, *13*, 1930; b) Y. Li, F. Mou, C. Chen, M. You, Y. Yin, L. Xu, J. Guan, *RSC Adv.* **2016**, *6*, 10697.

[26] E. Karshalev, B. Esteban-Fernández de Ávila, J. Wang, *J. Am. Chem. Soc.* **2018**, *140*, 3810.

[27] M. Enachi, M. Guix, V. Postolache, V. Ciobanu, V. M. Fomin, O. G. Schmidt, I. Tiginyanu, *Small* **2016**, *12*, 5497.

[28] Y. Wang, Z. Li, A. A. Solovev, G. Huang, Y. Mei, *RSC Adv.* **2019**, *9*, 29433.

[29] T. Luttrell, S. Halpegamage, J. Tao, A. Kramer, E. Sutter, M. Batzill, *Sci. Rep.* **2014**, *4*, 4043.

[30] K. Villa, A. Black, X. Domènech, J. Peral, *Sol. Energy* **2012**, *86*, 558.

[31] K. Huang, L. Chen, J. Deng, J. Xiong, *J. Nanomater.* **2012**, *2012*, 11.

[32] K. Almashhori, T. T. Ali, A. Saeed, R. Alwafi, M. Aly, F. E. Al-Hazmi, *New J. Chem.* **2020**, *44*, 562.

[33] A. Boonserm, C. Kruehong, V. Seithtanabutara, A. Artnaseaw, P. Kwakhong, *Appl. Surf. Sci.* **2017**, *419*, 933.

[34] X. Ma, A. C. Hortelao, A. Miguel-López, S. Sánchez, *J. Am. Chem. Soc.* **2016**, *138*, 13782.

ADVANCED
SCIENCE NEWS

www.advancedsciencenews.com

NANO · MICRO

small

www.small-journal.com

[35] S. Tang, F. Zhang, H. Gong, F. Wei, J. Zhuang, E. Karshalev, B. E.-F. de Ávila, C. Huang, Z. Zhou, Z. Li, L. Yin, H. Dong, R. H. Fang, X. Zhang, L. Zhang, J. Wang, *Sci. Rob.* **2020**, *5*, eaba6137.

[36] a) H. Choi, S. H. Cho, S. K. Hahn, *ACS Nano* **2020**, *14*, 6683; b) S. Hermanová, M. Pumera, *Chem. - Eur. J.* **2020**, *26*, 11085.

[37] V. Vaiano, O. Sacco, G. Di Capua, N. Femia, D. Sannino, *Water* **2019**, *11*, 1642.

[38] J. M. Macak, M. Zlamal, J. Krysa, P. Schmuki, *Small* **2007**, *3*, 300.

[39] H. Sopha, M. Krbal, S. Ng, J. Prikryl, R. Zazpe, F. K. Yam, J. M. Macak, *Appl. Mater. Today* **2017**, *9*, 104.

[40] J. A. Maciá-Agulló, A. Corma, H. Garcia, *Chem. - Eur. J.* **2015**, *21*, 10940.

[41] J. Ryu, S. H. Lee, D. H. Nam, C. B. Park, *Adv. Mater.* **2011**, *23*, 1883.

[42] A. J. Conneely, C. Bennett, G. M. O'Connor, T. Vollmerhausen, C. O'Byrne, G. Spence, D. Rowe, J. Victor, *International Congress on Applications of Lasers & Electro-Optics (ICALEO)* **2016**, *2016*, M604.

[43] Y. Lv, Z. Li, X. Zhou, S. Cheng, L. Zheng, *Sci. Total Environ.* **2020**, *749*, 142213.

[44] B. Krajewska, *J. Mol. Catal. B: Enzym.* **2011**, *68*, 262.

[45] R. Wu, X. Ou, R. Tian, J. Zhang, H. Jin, M. Dong, J. Li, L. Liu, *Nanoscale* **2018**, *10*, 20162.

[46] S. Borse, M. Temgire, A. Khan, S. Joshi, *RSC Adv.* **2016**, *6*, 56674.

[47] F. K.-M. Chan, K. Moriwaki, M. J. De Rosa, *Methods in Molecular Biology*, Humana Press, Totowa, NJ, New York, **2013**, Vol. *979*, p. 65.

[48] Y. H. Leung, X. Xu, A. P. Y. Ma, F. Liu, A. M. C. Ng, Z. Shen, L. A. Gethings, M. Y. Guo, A. B. Djurišić, P. K. H. Lee, H. K. Lee, W. K. Chan, F. C. C. Leung, *Sci. Rep.* **2016**, *6*, 35243.

[49] K. Pathakoti, S. Morrow, C. Han, M. Pelaez, X. He, D. D. Dionysiou, H.-M. Hwang, *Environ. Sci. Technol.* **2013**, *47*, 9988.

[50] Y. H. Leung, A. M. C. Ng, X. Xu, Z. Shen, L. A. Gethings, M. T. Wong, C. M. N. Chan, M. Y. Guo, Y. H. Ng, A. B. Djurišić, P. K. H. Lee, W. K. Chan, L. H. Yu, D. L. Phillips, A. P. Y. Ma, F. C. C. Leung, *Small* **2014**, *10*, 1171.

[51] Y. Cheng, H. Yang, Y. Yang, J. Huang, K. Wu, Z. Chen, X. Wang, C. Lin, Y. Lai, *J. Mater. Chem. B* **2018**, *6*, 1862.

[52] R. Zazpe, M. Knaut, H. Sopha, L. Hromadko, M. Albert, J. Prikryl, V. Gärtnerová, J. W. Bartha, J. M. Macak, *Langmuir* **2016**, *32*, 10551.

[53] H. Michalkova, Z. Skubalova, H. Sopha, V. Strmiska, B. Tesarova, S. Dostalova, P. Svec, L. Hromadko, M. Motola, J. M. Macak, V. Adam, Z. Heger, *J. Hazard. Mater.* **2020**, *388*, 122054.

[54] H. Yang, N. Fan, W. Luan, S. Tu, *Nanoscale Res. Lett.* **2009**, *4*, 344.

[55] N. Li, X. Zhang, S. Chen, X. Hou, Y. Liu, X. Zhai, *Mater. Sci. Eng.: B* **2011**, *176*, 688.

[56] A. M. Suhail, M. J. Khalifa, N. M. Saeed, O. A. Ibrahim, *Eur. Phys. J. Appl. Phys.* **2010**, *49*, 30601.

2106612 (8 of 8)